PCCP

ROYAL SOCIETY OF CHEMISTRY

REVIEW

View Article Online
View Journal | View Issue

Cite this: *Phys. Chem. Chem. Phys.*, 2026, **28**, 1016

Capric acid-driven three-phase antisolvent precipitation strategy for recycling metal and lixiviant from the leachate of spent sodium-ion batteries cathode

Yu Chen, *[a] Yaxue Shen,[a] Zhuojia Shi,[a] Zhenghui Liu, [c] Yanlong Wang,[b] Qi Liu[b] and Zheng Li [a]

Conventional methods for recycling metals from the leachate of spent sodium-ion batteries (SIBs) cathodes encounter several challenges, such as high energy consumption, complicated process and environmental pollution. Herein, a capric acid-driven three-phase antisolvent precipitation (CTAP) strategy is used for the low-energy and sustainable recovery of metal and lixiviant from the leachate associated with SIBs cathode vanadium phosphate sodium (NVP) and low-melting mixture solvents (LoMMSs). The CTAP strategy results in a three-phase precipitation, with the upper layer representing the capric acid phase, the middle layer consisting of the lixiviant phase, and the bottom layer comprising the solid phase. Through the CTAP strategy, capric acid achieves the antisolvent precipitation efficiencies of 86.8% for Na and 50.5% for V when applied to leachate from NVP and LoMMS polyethylene glycol 200:phytic acid; nevertheless, capric acid is ineffective in precipitating metals from leachate derived from LoMMSs that combine polyethylene glycol 200 with citric acid, benzoic acid, urea, or acetamide. Additionally, the LoMMSs using polyethylene glycol 200:phytic acid as the lixiviant achieve maximum leaching efficiencies of 99.1% for Na and 94.4% for V from NVP at a mild temperature of 80 °C over 24 hours, with a liquid-to-solid ratio of 200 after optimizing factors, such as hydrogen bond donors, molar ratios, temperature, time, liquid-to-solid ratio and scalability. This work provides an energy-saving, process-simplified and eco-friendly strategy for the separation of metals from SIBs leachate.

Received 3rd May 2025,
Accepted 25th November 2025

DOI: 10.1039/d5cp01667c

rsc.li/pccp

1. Introduction

The anticipated widespread usage of sodium-ion batteries (SIBs), driven by their high energy density, enhanced safety, and lower cost compared to lithium-ion batteries (LIBs),[1–7] is expected to lead to a substantial volume of spent SIBs in the near future due to their limited lifespan. Despite the low cost of Na, spent SIBs contain heavy metals, valuable elements, and rare minerals that can contribute to environmental pollution and natural resource waste; therefore, recovering these spent SIBs is crucial. The hydrometallurgical recovery of spent SIBs typically involves several steps: collection of spent SIBs, disassembly, metal leaching by solvents, separation of metals from the leachate, and metal refinement. Previous studies have primarily concentrated on the leaching of SIBs using solvents,[8–16] while the recovery of metals from the leachate has received comparatively less attention.

Antisolvent precipitation is a common strategy for separating metals from the SIBs leachate following hydrometallurgical dissolution.[8,10,12,14,16] For example, the precipitation efficiency from leachate using SIBs sodium-ion conductive ceramic powder (NZSP) and choline chloride:*p*-hydroxybenzyl alcohol (ChCl:PBA) follows this order: 1,8-diazabicyclo[5.4.0]undec-7-ene (DBU) > 1,5-diazabicyclo[4.3.0]non-5-ene (DBN) > ammonium hydroxide > hydrazine hydrate > water > hydrogen peroxide > triethylamine > engine oil > diisopropylamine, with the highest efficiency reaching 83.7%.[10] The order of metal precipitation from the leachate composed of polyethylene glycol 200:ascorbic acid and the SIBs cathode is as follows: lactic acid (80–85% in water) > DBU > *p*-tolualdehyde > tetrabutylammonium hydroxide > ammonium hydroxide > aniline > DBN > hydrogen peroxide > engine oil > phytic acid > diisopropylamine, with the highest efficiency reaching 81.6%.[14] The

[a] *Department of Chemistry and Material Science, Langfang Normal University, Langfang 065000, Hebei, China. E-mail: yuchen@iccas.ac.cn; Fax: +86-316-2112462; Tel: +86-316-2188211*
[b] *Hebei Regional Geological Survey institute, Langfang, 065000, China*
[c] *School of Pharmaceutical and Chemical Engineering, Taizhou University, Taizhou 318000, Zhejiang, China*

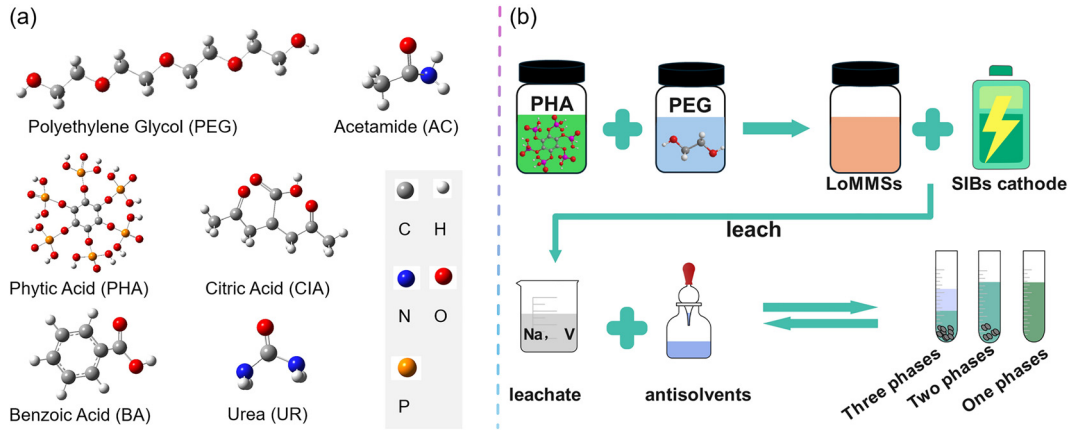

Fig. 1 Chemical structures of the components of LoMMSs investigated, including PHA, PEG, UR, AC, CIA, and BA (a). Flowchart illustrating the preparation process of LoMMSs, the leaching of the SIBs cathode, and the subsequent antisolvent precipitation (b).

application of the ionic liquid (IL) 1-butyl-3-methylimidazolium hexafluorophosphate ([BMIM][PF_6]) as an antisolvent yields a precipitation efficiency as high as 94.8% for the leachate containing the SIBs cathode sodium vanadium phosphate ($Na_3V_2(PO_4)_3$, NVP) and vegetable-/fruit-derived solvents.[8] When treating leachate containing SIBs cathode sodium iron phosphate and glucose:lactic acid, propanone and tetrahydrofuran achieve the highest and second-highest antisolvent precipitation efficiencies of 92.0% and 90.9%, respectively.[12] The application of ammonium hydroxide facilitates the precipitation of metal extracted from the leachate, yielding a maximum precipitation efficiency of 89.3% at room temperature from Prussian white and PEG200:-phytic acid (PEG:PHA).[16]

However, the aforementioned antisolvents (DBU,[10] lactic acid with a concentration of 80–85% in water,[14] [BMIM][PF_6],[8] propanone/tetrahydrofuran,[12] and ammonium hydroxide[16]), while providing optimal precipitation efficiency for SIBs, are problematic due to their corrosiveness, high cost, high flammability, and the need for complex separation. More importantly, the antisolvent precipitation methods reported are two-phase processes, indicating that the antisolvent and lixiviant are completely miscible. This results in a more complicated procedure and additional costs for the subsequent separation.

Here, we introduce the capric acid-driven three-phase antisolvent precipitation (CTAP) strategy to recover valuable metals from spent leachate containing SIBs cathodes and green lixiviant. The CTAP strategy offers advantages of high sustainability, low energy consumption, and simplicity when compared to the reported two-phase precipitation methods. NVP is chosen as a representative SIBs cathode because it contains hazardous heavy metals, like vanadium, which can leach into the environment, contaminating water and soil and posing a significant threat to human health due to its toxicity. Capric acid (CA) aligns with green chemistry principles due to its low toxicity, low cost, and good biodegradability, ensuring minimal environmental impact. LoMMSs are increasingly recognized as preferred green lixiviants, expanding the range of sustainable solvents, including ILs and deep eutectic solvents (DESs).[17] With their low vapor pressure, excellent thermal stability, and customizable solubility, LoMMSs are widely utilized in processes involving metal extraction, separation, and catalysis.[18–21] Fig. 1a presents the representative components of the studied LoMMSs, with PEG serving as the hydrogen-bond acceptor (HBA), while PHA, citric acid (CIA), benzoic acid (BA), urea (UR), and acetamide (AC) act as hydrogen-bond donors (HBD). The leaching and precipitation processes are illustrated in Fig. 1b. Abbreviations are also listed in Tables S1 and S2.

2. Material and methods

2.1. Materials and properties

The Li standard solution was provided by the National Standard (Beijing) Testing and Certification Co., Ltd. NVP was supplied by Shenzhen Kejing Zhida Technology Co., Ltd. Other chemicals, along with their names, abbreviations, purity levels, and suppliers, are provided in Table 2, which is consistent with our previous reports.[10,12,14] The pH was measured using the PHSJ-3F laboratory pH meter (±0.01). Density, surface tension and viscosity were respectively determined using the FA2104 electronic density balance (±0.0005 g cm^{-3}), QBZY-1 fully automatic surface tensiometer (±0.1 mN m^{-1}) and 8S digital viscometer (±0.01 mPa s). Each of the above properties was measured three times to ensure accuracy, and the average value was calculated. The electrochemical window was measured by cyclic voltammetry with platinum (Pt) as the counter electrode, glassy carbon (GC) as the working electrode and saturated calomel electrode (SCE) as the reference electrode. The infrared spectra (IR) and nuclear magnetic resonance (NMR) data were consistent with those reported with the same methods in our previous study.[22,23]

2.2. Leaching process

HBD and HBA were mixed at a specific molar ratio and stirred while heating at 60 °C until a clear and transparent solution was formed. The resulting mixture was then cooled to room temperature to obtain the LoMMSs. The HBA include PEG200.

The HBD were PHA, UR, CIA, BA and AC. The molar ratios of HBA to HBD were 2 : 1, 6 : 1, 10 : 1 and 14 : 1.

The LoMMSs and the NVP cathode were mixed and dissolved at a certain temperature for a specific period of time to obtain the LoMMS–NVP mixture. The resulting mixture was then centrifuged at 12 000 rpm for 20 min to separate the leachate and the residue. The leachate was diluted with 0.1 mol L^{-1} HNO_3 and analyzed for metal concentrations using inductively coupled plasma-optical emission spectrometry (ICP-OES). The leaching efficiency of the metals in the leachate was calculated according to eqn (1). The leaching temperatures were as follows: 25, 40, 60, 80, 100 and 120 °C. The leaching times were as follows: 0.017, 0.083, 0.17, 1, 6, 12, 24 and 36 h.

$$\eta_x = \frac{cm/\rho}{m_x} \times 100\% \quad (1)$$

In the equation, η_x is the leaching efficiency of specific metals in the leachate, c is the concentration of specific metals in the leachate measured by ICP-OES, m and ρ are the respective mass and density of the LoMMSs leaching specific metals, and m_x is the mass of specific metals added to the cathode material.

2.3. Antisolvent precipitation

First, the antisolvent and the leachate were mixed thoroughly using ultrasonication at a volume ratio of 1 : 1. Next, the resulting mixture was left to stand at room temperature for 48 h. Then, the solution after standing for three days was centrifuged at 12 000 rpm for 5 min, yielding three types of antisolvent precipitation results. Type 1: one single liquid phase; Type 2: one solid phase + one liquid phase; Type 3: two different liquid phases + one solid phase. The liquid phases from Type 2 and Type 3 were diluted 500-fold with 0.1 mol L^{-1} HNO_3, and the metal concentrations in the liquid were measured. The antisolvent precipitation efficiency was then calculated using eqn (2).

$$\eta_{x3} = \frac{\eta_{x1} - \eta_{x2}}{\eta_{x1}} \times 100\% \quad (2)$$

Here, η_{x1} and η_{x2} are the metal leaching efficiencies in the leachate before and after the addition of the antisolvent, respectively; η_{x3} is the efficiency of metal precipitation from the leachate facilitated by the antisolvent.

The two different liquid phases from Type 3 were separated to obtain the recovered antisolvent and the recovered LoMMSs. The recovered LoMMSs were then used to leach the NVP cathode following the same procedure as in the initial leaching process, and the corresponding metal leaching efficiency was obtained. The recovered antisolvent was applied to separate metals from the above leachate following the same antisolvent precipitation process, and the metal precipitation efficiency of the recovered antisolvent was determined. The above leaching and antisolvent precipitation processes using the recovered LoMMSs and the recovered antisolvent constituted the recycling process of the LoMMSs and the antisolvent.

3. Results and discussion

3.1. Effect of HBD

The studied HBD in LoMMSs for leaching metal from NVP include PHA, CIA, BA, UR and AC, with PEG fixed as the HBA in a mole ratio of HBA : HBD = 6 : 1 (Fig. 2a and Table 1). Among the five types of LoMMSs studied, the leaching efficiency for Na consistently outperforms that of V. The leaching efficiency of Na is the highest with PEG:PHA (96.4%), followed by PEG:CA (26.7%), PEG:BA (8.9%), PEG:UR (7.1%), and PEG:AC (7.1%). For V, the efficiencies are PEG:PHA (80.6%), PEG:CIA (19.7%), PEG:AC (2.4%), PEG:UR (1.6%), and PEG:BA (0.8%).

The results indicate that PEG:PHA demonstrates the highest leaching efficiency for both Na and V among all LoMMSs investigated, suggesting that the leaching of Na and V can be effectively regulated through the choice of HBD. This finding underscores the critical role of HBD in metal leaching from SIBs. Therefore, PEG:PHA is selected as the representative LoMMSs for subsequent investigation. The highest leaching efficiency by PEG:PHA might be ascribed to the fact that PHA contains multiple phosphate groups, which may coordinate with metal ions to facilitate their dissolution. Na and V may be strongly electrostatically attracted to these phosphorus ions in

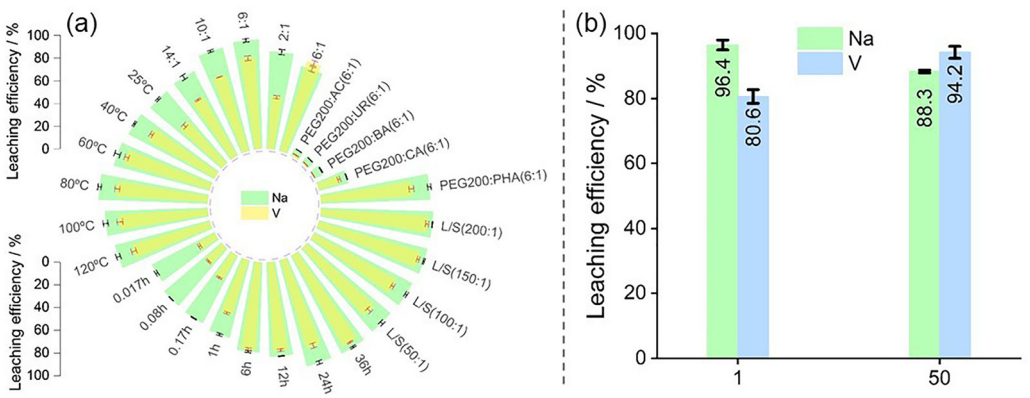

Fig. 2 Effect of HBD, molar ratio, temperature, time and *L*/*S* on the leaching efficiency from NVP by LoMMSs (a). Effect of scalability on the concentration and leaching efficiency from NVP by LoMMS PEG : PHA (6 : 1) (b).

Table 1 Effect of HBD, molar ratio, temperature, time, liquid-to-solid ratio, and scalability on the leaching efficiency of Na and V from NVP by LoMMSs

Variable	Condition	η_{Na}/%	η_{V}/%
HBD	PEG : PHA (6 : 1)	96.4 ± 1.5	80.6 ± 2.1
	PEG : CIA (6 : 1)	26.7 ± 0.3	19.7 ± 1.2
	PEG : BA (6 : 1)	8.9 ± 0.4	0.8 ± 0.1
	PEG : UR (6 : 1)	7.1 ± 0.2	1.6 ± 0.1
	PEG : AC (6 : 1)	7.1 ± 0.2	2.4 ± 0.1
Molar ratio/mol mol^{-1}	PEG : PHA (2 : 1)	86.0 ± 2.3	46.3 ± 1.3
	PEG : PHA (6 : 1)	96.4 ± 1.5	80.6 ± 2.1
	PEG : PHA (10 : 1)	94.0 ± 1.0	70.2 ± 0.1
	PEG : PHA (14 : 1)	83.8 ± 2.1	60.2 ± 0.7
Temperature/°C	25	82.6 ± 0.9	49.6 ± 1.6
	40	85.4 ± 0.7	67.7 ± 1.3
	60	87.4 ± 2.5	78.7 ± 1.8
	80	96.4 ± 1.5	80.6 ± 2.1
	100	90.9 ± 2.1	78.3 ± 2.5
	120	86.5 ± 1.8	71.9 ± 2.2
Time/h	0.017	62.2 ± 1.1	17.3 ± 1.0
	0.083	66.4 ± 0.2	19.6 ± 0.7
	0.17	67.3 ± 0.4	25.0 ± 0.7
	1	70.4 ± 1.0	50.4 ± 0.9
	6	79.4 ± 1.0	77.3 ± 1.3
	12	83.4 ± 0.3	78.1 ± 1.1
	24	96.4 ± 1.5	80.6 ± 2.1
	36	97.1 ± 0.8	92.1 ± 0.5
liquid-to-solid ratio/g g^{-1}	50 : 1	96.4 ± 1.5	80.6 ± 2.1
	100 : 1	97.5 ± 1.0	83.5 ± 1.2
	150 : 1	98.9 ± 0.6	93.5 ± 1.1
	200 : 1	99.1 ± 0.3	94.4 ± 1.4
Scalability	1	96.4 ± 1.5	80.6 ± 2.1
	50	88.3 ± 0.4	94.2 ± 1.8

PHA. In addition, the hydrogen from the hydroxyl group in PEG exhibits a strong attraction to the phosphorus ions.

3.2. Effect of mole ratios

The leaching efficiencies of Na in PEG : PHA 2 : 1, 6 : 1, 10 : 1 and 14 : 1 (Fig. 2a and Table 1) are 86.0%, 96.4%, 94.0% and 83.8%, respectively. The V leaching efficiencies are 46.3%, 80.6%, 70.2% and 60.2%. The leaching efficiencies for both Na and V initially increase with higher mole ratios, peaking at PEG : PHA (6 : 1) before gradually declining. The leaching efficiencies of Na and V significantly increase from PEG : PHA (2 : 1) to PEG : PHA (6 : 1), while the leaching efficiencies of Na and V slightly decrease from PEG : PHA (6 : 1) to PEG : PHA (14 : 1). Furthermore, the Na leaching efficiency is higher than the V leaching efficiency. This means that both PEG and PHA are very important for the metal leaching. Therefore, PEG : PHA (6 : 1) is selected as the mole ratio for the following optimization.

3.3. Effect of temperature

To investigate the impact of temperature on the metal leaching from NVP using PEG : PHA (6 : 1), six temperature points are selected: 25 °C, 40 °C, 60 °C, 80 °C, 100 °C and 120 °C (Fig. 2a and Table 1). The results indicate that the leaching efficiencies for Na and V initially increase, reaching maximum values at 80 °C; the leaching efficiencies for Na and V are respectively 96.4% and 80.6% before gradually declining at 100–120 °C. Increasing the temperature can reduce the viscosity of LoMMSs, improving the mass-transfer rate and promoting the diffusion of metal ions from the solid phase to the liquid phase. It is consistent with the general understanding that reduced viscosity improves ion mobility and accelerates dissolution kinetics. However, as the temperature rises from 100 °C to 120 °C, the concentrations and leaching efficiencies of both Na and V decline. This decline may be attributed to the thermal instability of PHA, which compromises its coordination capability and overall leaching performance.

3.4. Effect of time

Eight time points (*i.e.*, 0.017 h, 0.083 h, 0.17 h, 1 h, 6 h, 12 h, 24 h, 36 h) are selected to study the effect of time on metal leaching from NVP by PEG : PHA (6 : 1) (Fig. 2a and Table 1). The results show that the leaching efficiencies of both Na and V gradually increase with time. Interestingly, the leaching efficiency of Na is 62.2% when the time is 0.017 h, showing the high selectivity of LoMMSs to Na. When the time is 36 h, the leaching efficiencies of Na and V are high. To reduce the leaching time, we chose 24 h as the optimized time. We fixed the time at 24 h for the subsequent experiments.

3.5. Effect of liquid-to-solid ratio

Liquid-to-solid ratios (50 : 1, 100 : 1, 150 : 1, and 200 : 1 g g^{-1}) are investigated. For this purpose, 0.1 g of NVP is kept constant, and the corresponding amounts of LoMMSs (5 g, 10 g, 15 g, and 20 g) are selected, respectively. Fig. 2a and Table 1 show that the leaching efficiencies of Na and V could be enhanced by increasing the liquid-to-solid ratios from 50 : 1 to 200 : 1. For example, the Na leaching efficiency could increase from 96.4% to 99.1%, and the V leaching efficiency could increase from 80.6% to 94.4%. The mass of LoMMSs is positively correlated with the leaching efficiency of metals. In a word, with the increase in the liquid-to-solid ratios, Na and V are more easily recovered simultaneously.

3.6. Effect of scalability

The scale factors of the experiment are selected as 1 and 50 to explore the feasibility for industrial production (Fig. 2b and Table 1). When the scale factor was 1, the leaching efficiencies of Na and V are 96.4% and 80.6%, respectively. This indicates that the LoMMSs can simultaneously and efficiently leach Na and V. When the scale factor is 50, the leaching efficiencies of Na and V are 88.3% and 94.2%, respectively. LoMMSs still maintain a high efficiency for Na and V in SIBs. Table 1 shows that the effect of scalability on leaching efficiency is very low. Therefore, this work demonstrates promising prospects for industrial application.

3.7. Comparison

PEG : PHA (6 : 1) could achieve a Li recovery efficiency of 96.4% and an Na recovery of 80.6% for NVP cathodes at 80 °C for 24 h with a liquid-to-solid ratio of 200, outperforming many other green solvent systems reported previously (Table 3). GLU : LA (1 : 9) systems yield 86.1% Li and 96.0% Na recovery but show limited performance on other cathode materials.[12] Vegetable

Table 2 Summary of the chemical names, abbreviations, purity, suppliers, and the precipitation efficiency by antisolvents[a]

Entry	Antisolvents or other chemicals	Abbre.	Purity	Suppliers	Prec.	η_{Na}/%	η_V/%
1	1,4-Dioxane	DX	99.0%	Rhnwa	×		
2	1,5-Diazabicyclo[4.3.0]non-5-ene	DBN	98%	Innochem	×		
3	1,8-Diazabicyclo[5,4,0]undec-7-ene	DBU	99.0%	McLean	×		
4	*n*-Propanol	PrOH	99.0%	Aladdin	√(2)	47.6 ± 0.7	42.4 ± 0.2
5	Collodion	COL	≥5.0%	Tianjin Damao	×		
6	2-Methylbut-3-yn-2-ol	MBY	98%	Innochem	×		
7	5-Norbornene-2-methanol	NBM	98.0%	Ark Pharm	×		
8	5-Norbornene-2-carboxylic acid	NBCA	99.0%	Aladdin	×		
9	*N*,*N*-Dimethylformamide	DMF	≥99.5%	Tianjin Bohua	√(2)	79.3 ± 0.6	99.5 ± 0.3
10	*N*-Methylpyrrolidone	NMP	≥99.0%	Aladdin	√(2)	50.2 ± 0.5	48.0 ± 0.6
11	*N*-Methylacetamide	NMA	>99.0%	Tokyo Chemical Industry	√(2)	51.4 ± 0.4	47.7 ± 0.3
12	Ammonium hydroxide	NH_4OH	25–28% in H_2O	Aladdin	√(2)	94.4 ± 0.1	98.6 ± 0.1
13	Aniline	$PhNH_2$	≥99.5%	Tianjin Guangfu	×		
14	Phenol	PhOH	≥99.0%	Chemical Reagent	×		
15	Benzyl alcohol	BnOH	99.0%	Innochem	√(2)	53.8 ± 1.1	48.3 ± 0.1
16	Pyridine	PY	>99.0%	Shanghai Chemical Reagent	×		
17	Acetic acid	ACA	≥99.5%	Tianjin Bohua	√(2)	55.8 ± 1.2	66.4 ± 0.5
18	Nitric acid	HNO_3	65–68% in H_2O	Tianjin Damao	√(2)	39.0 ± 1.3	31.3 ± 0.2
19	Edible oil	EO	NA	SuperMarket	×		
20	Glycerol	GLY	≥98.0%	Sinopharm	×		
21	Propanone	PP	>99.6%	Tianjin Jindong Tianzheng	√(2)	38.6 ± 0.4	28.2 ± 0.3
22	Dichloromethane	DCM	99.9%	Innochem	×		
23	Silicone oil	SOI	NA	Innochem	×		
24	Ethyl acetate	EAC	99.0%	Aladdin	×		
25	Dimethyl sulfoxide	DMSO	AR	Tianjin Chemical Reagent	√(2)	53.1 ± 0.9	46.9 ± 0.3
26	Levulinic acid	LEA	98.0%	Innochem	×		
27	Isopropanol	IPA	99.5%	Aladdin	√(2)	49.1 ± 0.4	42.0 ± 0.2
28	1-Butyl-3-methylimidazolium hexafluorophosphate	$BMIMPF_6$	97.0%	McLean	×		
29	Propanoic acid	PA	99.0%	Tianjin Guangfu	×		
30	Tetrabutyl titanate	TBT	≥98.0%	Tianjin Bohua	×		
31	Cyclopentane	cPen	96.0%	Aladdin	×		
32	Epichlorohydrin	ECH	99.0%	Tianjin No. 6 Chemical	×		
33	Engine oil	ENO	NA	Mobil	×		
34	Toluene	PhMe	≥99.5%	Tianjin Chemical Reagent	×		
35	Methyl alcohol	MeOH	≥99.9%	Tianjin Bohua	√(2)	57.7 ± 0.9	52.2 ± 0.3
36	Methyl *tert*-butyl ether	MTBE	>99.0%	Aladdin	×		
37	Polyethylene glycol 200	PEG	NA	Innochem	×		
38	Polyethylene glycol 600	PEG600	NA	Tianjin Tianli	×		
39	Phytic acid	PHA	70% in H_2O	Aladdin	×		
40	Benzene	PhH	≥99.5%	Tianjin Chemical Reagent	√(3)	73.4 ± 1.6	91.9 ± 0.9
41	Lactic acid	LA	85–90% in H_2O	Innochem	×		
42	Diisopropylamine	DIPA	≥99.0%	Innochem	×		
43	Trichloromethane	TCM	≥99.0%	Tianjin Jindong Tianzheng	×		
44	Triethylamine	TEA	99.0%	Aladdin	×		
45	Triethanolamine	TEOA	≥85.0%	Tianjin Dongli Tianda	×		
46	Naphtha	NA	99%	Tianjin Chemical Reagent	×		
47	Hydrazine hydrate	HH	80.0% in H_2O	Tianjin Dingshengxin	×		
48	Tetrabutylammonium hydroxide	TBAH	25% in H_2O	Aladdin	√(2)	54.7 ± 1.2	44.6 ± 0.6
49	Hydrobromic acid	HBr	40% in H_2O	Aladdin	√(2)	76.4 ± 0.3	94.6 ± 0.0
50	Cyclohexane	cHex	99.5%	Tianjin Chemical Reagent	×		
51	Tetrahydrofuran	THF	99.0%	Tianjin Bohua	√(2)	18.7 ± 2.8	6.3 ± 0.5
52	Propylene carbonate	PCA	>98.0%	Aladdin	√(2)	48.2 ± 2.0	40.5 ± 0.2
53	Tetrabutylammonium hydroxide	TBAH	40% in MeOH	Innochem	√(2)	66.6 ± 0.4	90.2 ± 0.0
54	Formic acid	FA	98.0%	Aladdin	√(2)	55.2 ± 0.3	60.7 ± 0.2
55	Ethanol	EtOH	99.9%	Innochem	√(2)	49.3 ± 1.1	43.0 ± 0.2
56	Diethyl ether	DE	≥99.0%	Tianjin Jindong Tianzheng	×		
57	Ethylene glycol	EG	99.0%	Aladdin	√(2)	56.4 ± 0.1	49.5 ± 0.2
58	Ethylene glycol diethyl ether	EGDE	>99.0%	Beijing Chemical Reagent	√(2)	16.7 ± 1.3	0.5 ± 0.7
59	Acetonitrile	MeCN	>99.0%	Tianjin Bohua	√(2)	55.5 ± 1.2	49.5 ± 0.5
60	Ethyl vinyl ether	EVE	>98.0%	Adamas	×		
61	*n*-Butyl acetate	BuOAc	>99.0%	Tianjin Second Chemical	×		
62	Acetic anhydride	AA	≥98.5%	Tianjin Chemical Reagent	×		
63	Hydrogen peroxide	H_2O_2	30.0% in H_2O	Tianjin Chemical Reagent	√(2)	57.4 ± 1.3	51.7 ± 0.3
64	Acetylacetone	AAC	99.0%	Aladdin	×		
65	1-Octyl-3-methylimidazolium hexafluorophosphate	$OMIMPF_6$	95.0%	McLean	×		
66	1-Butyl-3-methylimidazolium tetrafluoroborate	$BMIMBF_4$	99%	Innochem	×		
67	Polyethylene glycol 300	PEG300	NA	Innochem	×		

Table 2 (*continued*)

Entry	Antisolvents or other chemicals	Abbre.	Purity	Suppliers	Prec.	η_{Na}/%	η_V/%
68	Capric acid	CA	99.0%	Innochem	√(3)	86.8 ± 3.1	50.5 ± 0.6
69	*n*-Pentane	PEN	97.0%	Aladdin	×		
70	Water	H_2O	distilled water	Self-made	√(2)	63.5 ± 0.6	51.8 ± 0.5
71	Benzoic acid	BA	99.5%	Innochem			
72	Acetamide	AC	99.0%	Aladdin			
73	Citric acid	CIA	99.0%	Innochem			
74	Urea	UR	99.0%	Aladdin			

[a] Entries 1–70 are classified as antisolvents, while other entries are not. The symbol √ denotes precipitation, while × indicates no precipitation observed. The numbers 2 and 3 in parentheses indicate two phases and three phases, respectively.

and fruit solvents (VFSs) demonstrate much lower efficiencies (59.1% for Li, 52.4% for Na).[8] Other systems, like ChCl:CAT and PEG:AA, demonstrate either lower selectivity or lower recovery efficiencies under similar conditions.[14] Our work therefore demonstrates a competitive or superior leaching performance under mild conditions (80 °C, 24 h), suggesting that the proposed PEG:PHA system offers a green and effective alternative for selective metal recovery from LIBs and SIBs cathodes.

3.8. Antisolvent precipitation

Seventy different antisolvents (Table 2 and Tables S2, S3) are screened for the precipitation of metals from the leachate. A total of 26 antisolvents successfully demonstrated precipitation, while the remaining 44 do not yield any detectable precipitation. The 26 effective antisolvents include NH_4OH, CA, DCM, HBr, PhH, TBAH, H_2O, MeOH, H_2O_2, EG, ACA, MeCN, FA, TBAH, BnOH, DMSO, NMA, NMP, EtOH, IPA, PCA, PrOH, HNO_3, PP, THF and EGDE. The precipitation results for the 70 different antisolvents could be categorized into three types: Type 1, Type 2, and Type 3, as described below.

Type 1. 1 phase = 1 liquid phase

Type 2. 2 phases = 1 liquid phase + 1 solid phase

Type 3. 3 phases = 2 liquid phases + 1 solid phase

In the first type (Type 1), the single liquid consists of a mixture of leachate and antisolvent, indicating an inability to produce precipitated solids. In Type 2, the precipitation products constitute a single solid phase, while the lixiviants within the leachate and antisolvents combine to form a single liquid phase, resulting in two distinct phases. The antisolvents associated with Type 2 include 24 different types, such as NH_4OH, DCM, HBr, TBAH, H_2O, MeOH, H_2O_2, EG, ACA, MeCN, FA, TBAH, BnOH, DMSO, NMA, NMP, EtOH, IPA, PCA, PrOH, HNO_3, PP, THF and EGDE. This demonstrates that NH_4OH exhibits the highest antisolvent efficiency, achieving 94.4% for Na and 98.6% for V. Additionally, H_2O serves as a cost-effective and sustainable antisolvent for the subsequent recovery of dissolved cathode materials from leachates, achieving high efficiency levels of 63.5% for Na and 58.1% for V at room temperature. Despite these advantages, the regeneration of the antisolvents and lixiviant in Type 2 is challenging and may involve complex and energy-intensive processes.

In contrast, Type 3 involves the lixiviant and antisolvent existing as two separate liquid phases, while the precipitation products form one solid phase, resulting in three distinct phases. The relevant antisolvents in this case are limited to CA and PhH, demonstrating Na and V precipitation efficiencies of 86.8%/73.4% and 50.5%/91.9%, respectively. However, PhH is toxic and carcinogenic, making it unfavourable and impractical for green and sustainable precipitation, even though its antisolvent precipitation efficiency is slightly higher than that of CA. On the other hand, CA serves as a relatively inexpensive yet more environmentally friendly solvent compared to PhH. This precipitation method utilizing CA exemplifies the CTAP strategy employed in this study, facilitating the straightforward

Table 3 Comparison of leaching efficiency

Green solvent	Mole ratio	Plus	Cathode	T/°C	t/h	L/S/g g^{-1}	η_{Li}/%	η_{Na}/%	η_V/%	η_{Fe}/%	η_{Mn}/%	η_{Ni}/%	Ref.
PEG : PHA	6 : 1		NVP	80	24	50		96.4	80.6				This work
PEG : PHA	14 : 1		NMF	80	24	50		94.7		21.6	9.6		16
GLU : LA	1 : 9		NVP	80	24	50		86.1	96.0				12
GLU : LA	1 : 9		NMF	80	24	50		77.9		0.7	0.5		12
GLU : LA	1 : 9		NFP	80	24	50		92.8		41.2			12
VFSs	—		NVP	80	24	50		59.1	52.4				8
PEG : AA	14 : 1		NMF	80	24	50		63.5		0.5	0.2		14
ChCl : CAT	1 : 1	35 wt% H_2O	NVP	80	24	50		81.7	29.8				10
ChCl : CAT	1 : 1	35 wt% H_2O	NVP	80	24	50		84.2		0.8			10
Val : LA	1 : 12		LCO	80	24	50	64.1					8.7	24
Val : LA	1 : 12		LCO	120	24	50	100.0					48.4	24
ChCl : CuCl : LA	1 : 1 : 4		LCO	100	0.5	25	100.0					96.3	25
PEG : AA	6 : 1		LCO	80	24	50	34.6					39.2	26
PEG : PHA	1 : 1		LCO	80	24	50	96.9					98.7	27
CAA : EtOH	1 : 1	O_2	LFP	70	6	100	100.0			0.3			28
ChCl : EG	1 : 2		LCO	180	24	50	89.8					50.3	29

separation of the lixiviant, antisolvent, and precipitation products. With the increase in the leaching cycles, the leaching efficiencies of Na and V gradually decrease (Table S4). The leaching efficiency of Na continuously declines from 96.4% to 15.6%, while that of V decreases from 80.6% to 23.8%. As the LoMMSs are reused, their ability to complex and transfer metal ions progressively weakens. The antisolvent precipitation efficiencies for Na and V reach 86.8% and 50.5%, respectively, indicating that the system exhibits a relatively high metal separation efficiency at the early stage. However, with the repeated use of the antisolvent, the metal precipitation efficiency declines significantly. The precipitation efficiency for V decreases sharply from 50.5% to 2.7%, indicating a significant downward trend.

3.9. Physical properties

The physical properties are characterized as illustrated in Fig. 3, 4 and Tables S5, S6. The viscosities of PEG, PHA, LoMMS, and leachate are 42.0, 918.0, 447.0, and 478.2 mPa s, respectively (Fig. 3a and Fig. S5). The slightly higher viscosity of the leachate compared to that of the LoMMS indicates that NVP is effectively dissolved by the LoMMSs. The density and surface tension trends align with viscosity. The leachate has a higher pH (0.2) than the LoMMSs (0.06), likely due to the acid–base interactions between the LoMMSs and NVP. The LoMMSs, their components, and the leachate exhibit no flammability (Fig. 3b), indicating the safe recovery of spent SIBs cathodes. The electrochemical window of the LoMMSs narrows after the leaching of the spent SIBs cathodes, as the cathodic limit increases while the anodic limit decreases (Fig. 3c). This suggests that the reducing ability increases from the LoMMSs to the leachate, which contradicts the expected redox reactions between NVP and the LoMMSs, as such reactions would typically diminish the reducing power of the LoMMSs following metal leaching. This is in agreement with the conclusions drawn from the IR spectra and NMR analysis, which suggest that physical processes or coordination interactions are the primary driving forces behind the ability of LoMMSs to dissolve SIB cathodes, as indicated by the minimal change and slight shifts observed (Fig. 4a and c). The IR and NMR results for the LoMMSs before and after heating at 80 °C for 24 hours are nearly identical (Fig. 4b and c), indicating the high thermal stability of the LoMMSs.

NVP, residue, and precipitation are further analyzed using SEM, EDS, and XRD. SEM (Fig. 5a) illustrates that the NVP cathode predominantly exhibits porous spherical shapes with diameters exceeding 10 μm; however, after dissolution, the morphology transforms into an irregular structure with diameters significantly reduced to less than 3 μm. This suggests that the LoMMSs may dissolve the NVP cathode primarily from the exterior. Furthermore, as indicated by the EDS data in Fig. 5b, leaching NVP ($Na_{1.64}V$) with LoMMSs results in a

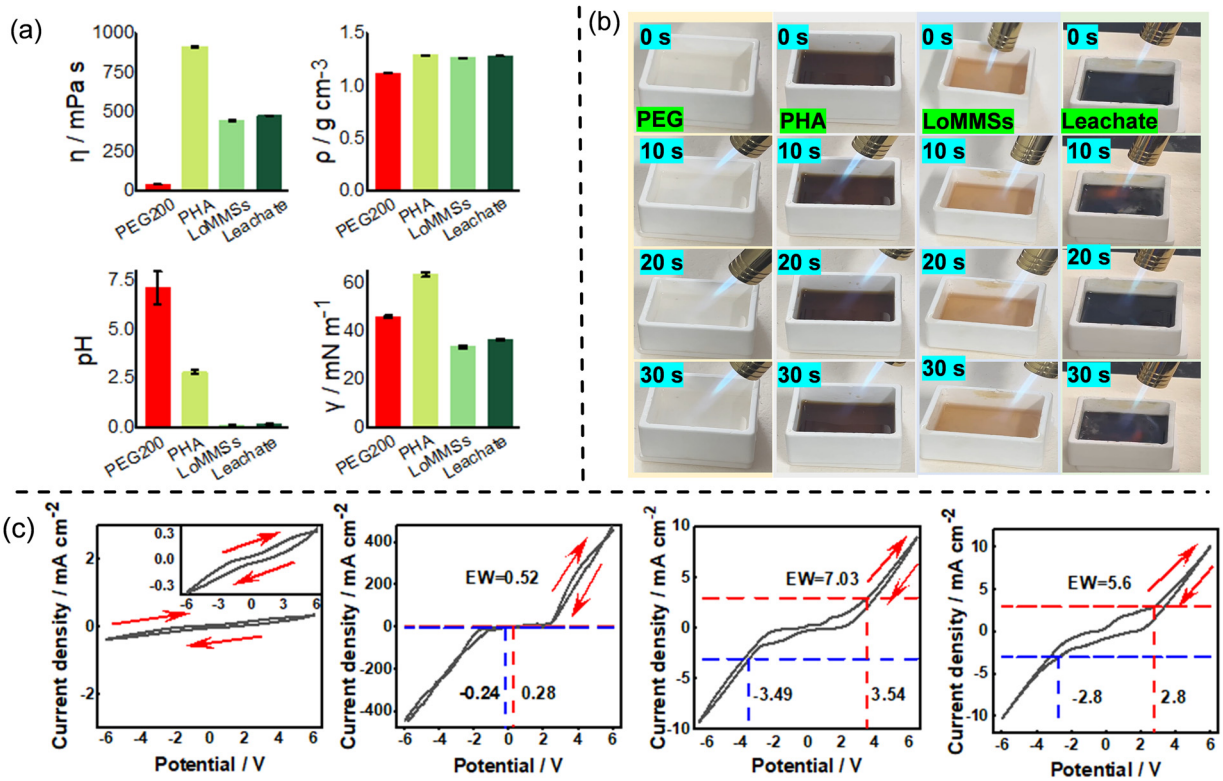

Fig. 3 Physical properties of viscosity, density, pH and surface tension (a). Combustion of PEG, PHA, PEG : PHA (6 : 1), leachate (80 °C, 24 h, 0.1 g NVP, and 5 g of LoMMS PEG:PHA) (b). Cyclic voltammograms of PEG, PHA, PEG : PHA (6 : 1), leachate (from left to right) with the parameters of a 100 mV s^{-1} scan rate, Pt counter electrode, GC working electrode, SCE reference electrode, and 3 mA cm^{-2} cutting-off current density (c).

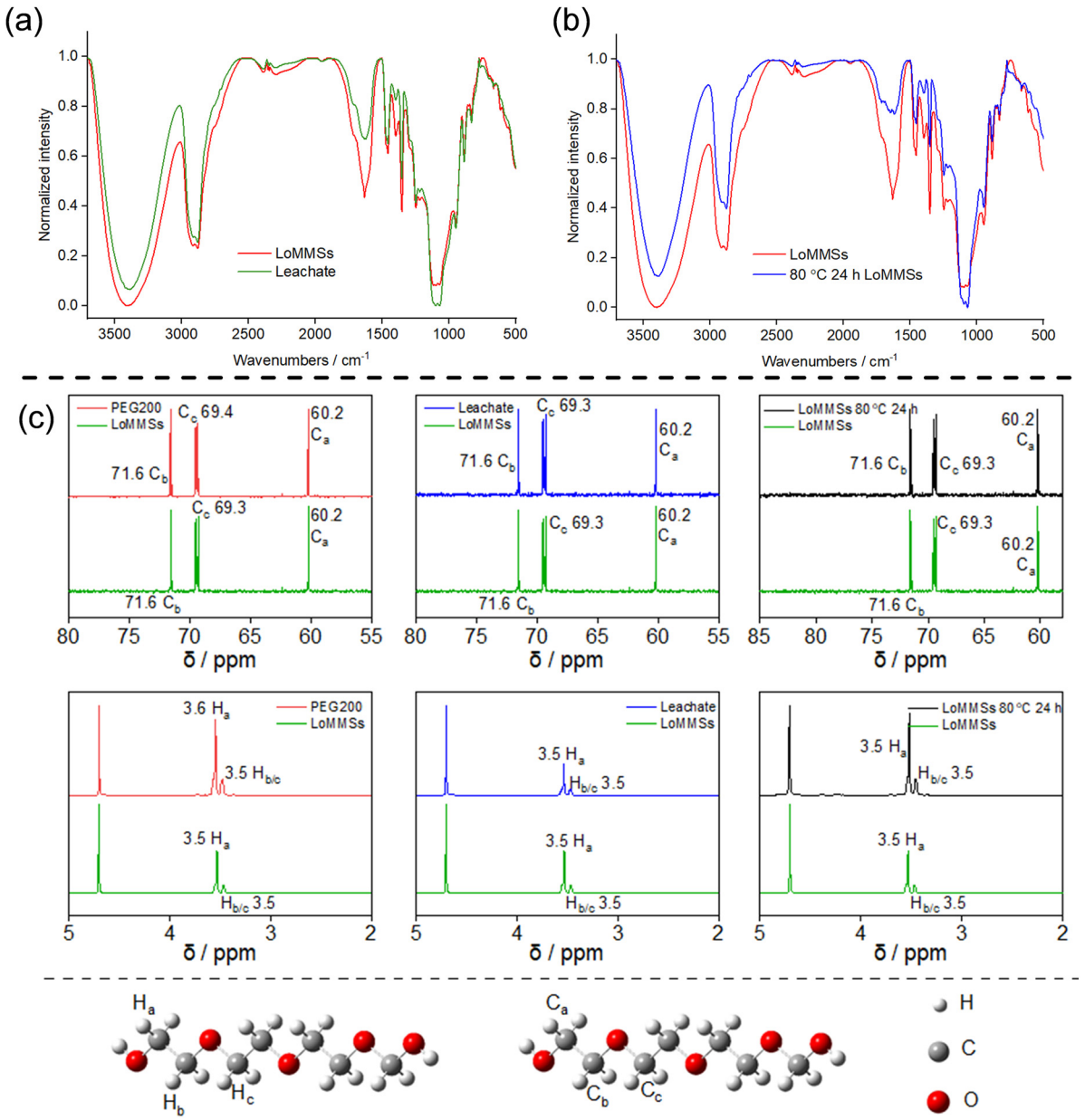

Fig. 4 IR spectra of LoMMS PEG : PHA (6 : 1) and leachate (a). LoMMSs before and after heating at 80 °C for 24 h (b). NMR spectra in D_2O (c).

substantial decrease in the Na content in the residue ($Na_{0.42}V$). Using an antisolvent to precipitate metals from the leachate also causes a reduction in the Na content ($Na_{0.06}V$). Fig. 5c reveals the XRD patterns of the residue and precipitate, which show significant differences compared to those of NVP. NVP is crystalline, whereas the residue and precipitate are non-crystalline.

4. Conclusions

In summary, the CTAP strategy is employed for the energy-efficient, process-simplified and sustainable precipitation of metals and lixiviants from the leachate related to SIBs cathode NVP and LoMMSs. The CTAP strategy consists of three phases: the upper antisolvent layer, the middle lixiviant layer, and the bottom solid layer. Employing the CTAP strategy, CA, among 70 different antisolvents, demonstrates precipitation efficiencies of 86.8% for Na and 50.5% for V at room temperature when applied to the leachate from NVP and LoMMS PEG:PHA. While BE exhibits three-phase antisolvent precipitation, its toxicity and carcinogenicity make it unsuitable for widespread application as an antisolvent. No precipitation is observed for the leachate containing the other four LoMMSs, namely PEG:UR, PEG:BA, PEG:AC, and PEG:CIA. Six factors are investigated, including hydrogen-bond donors, molar ratios, temperature, time, liquid-to-solid ratio, and scalability, resulting in optimal leaching efficiencies of 99.1% for Na and 94.4% for V from NVP

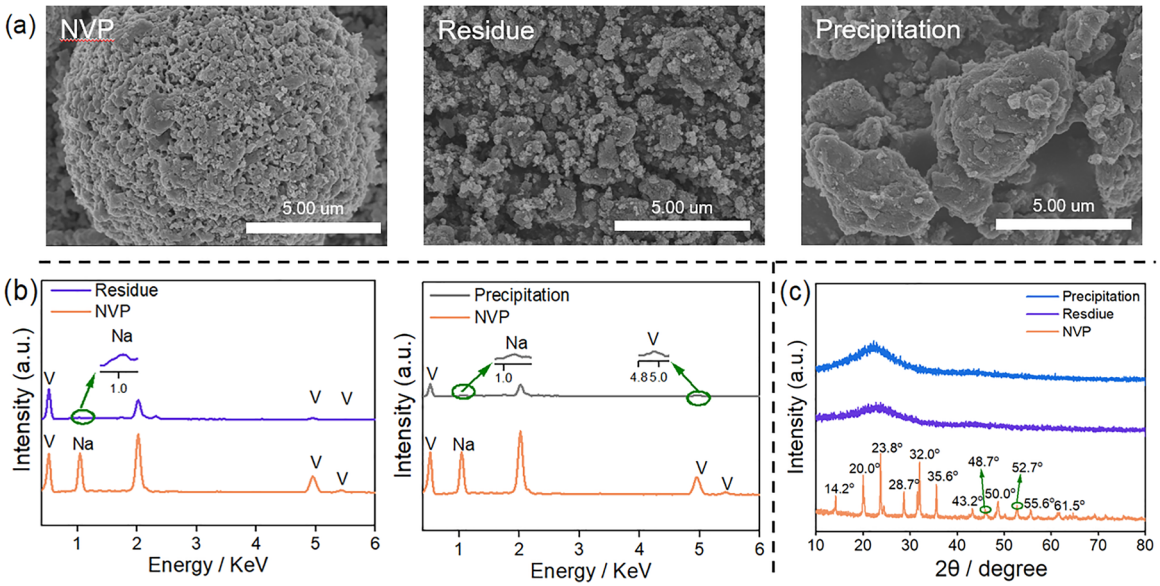

Fig. 5 SEM (a), EDS (b) and XRD (c) of the NVP, residues and precipitation.

at a mild temperature of 80 °C over a period of 24 h, with a liquid-to-solid ratio of 200. The underlying mechanism of antisolvent precipitation will be explored further in upcoming studies.

Author contributions

Yu Chen: conceptualization, supervision, writing – original draft, writing – review & editing, project administration, funding acquisition. Yaxue Shen & Zhuojia Shi: writing – original draft, writing – review & editing, investigation, data curation. Yanlong Wang, Qi Liu, Zheng Li & Zhenghui Liu: investigation, data curation.

Conflicts of interest

The authors declare no competing financial interests.

Data availability

The data supporting this article (cost, abbreviations, purity, metal concentration for precipitation, solvent reusability, and properties) have been included as part of the supplementary information (SI). Supplementary information is available. See DOI: https://doi.org/10.1039/d5cp01667c.

Acknowledgements

This work was supported by the Natural Science Foundation of Hebei Province/S&T Program of Hebei (B2024408022), the Fundamental Research Funds for the Universities in Hebei Province (JYT202502), the Natural Science Foundation of Hebei Province/S&T Program of Hebei (B2024408003), and the National College Students' Innovation and Entrepreneurship Training Program Project Fund of Langfang Normal University (202510100002).

References

1 J. Wang, Y.-F. Zhu, Y. Su, J.-X. Guo, S. Chen, H.-K. Liu, S.-X. Dou, S.-L. Chou and Y. Xiao, Routes to high-performance layered oxide cathodes for sodium-ion batteries, *Chem. Soc. Rev.*, 2024, **53**, 4230–4301.
2 W. Hu, M. Yang, T. Fan, Z. Li, Y. Wang, H. Li, G. Zhu, J. Li, H. Jin and L. Yu, A simple, efficient, fluorine-free synthesis method of MXene/$Ti_3C_2T_x$ anode through molten salt etching for sodium-ion batteries, *Battery Energy*, 2023, **2**, 20230021.
3 D. Zhang and H. Xu, Nickel modified TiO_2/C nanodisks with defective and near-amorphous structure for high-performance sodium-ion batteries, *Battery Energy*, 2024, **3**, 20230032.
4 Z. Zhang, Y. Du, Q.-C. Wang, J. Xu, Y.-N. Zhou, J. Bao, J. Shen and X. Zhou, A Yolk-Shell-Structured $FePO_4$ Cathode for High-Rate and Long-Cycling Sodium-Ion Batteries, *Angew. Chem., Int. Ed.*, 2020, **59**, 17504–17510.
5 C. Wang, H. Long, L. Zhou, C. Shen, W. Tang, X. Wang, B. Tian, L. Shao, Z. Tian, H. Su and K. Xie, A multiphase sodium vanadium phosphate cathode material for high-rate sodium-ion batteries, *J. Mater. Sci. Techonol.*, 2021, **66**, 121–127.
6 S. Lin, H. Zhang, C. Shu, W. Hua, X. Wang, Y. Zhao, J. Luo, Z. Tang, Y. Wu and W. Tang, Research Progress and Perspectives on Pre-Sodiation Strategies for Sodium-Ion Batteries, *Adv. Funct. Mater.*, 2024, **34**, 2409628.
7 M. Xu, M. Liu, Z. Yang, C. Wu and J. Qian, Research progress on presodiation strategies for high energy sodium-ion batteries, *Acta Phys. Chim. Sin.*, 2022, **39**, 2210043.

8 Y. Chen, Z. Yang, M. Zhao, X. Wang, D. Dong, Z. Niu, J. Dong and Z. Li, Green strategy for recycling spent all-solid-state sodium-ion batteries and kitchen waste using biomass-based vegetable-/fruit-derived solvents, *Sustainable Energy Fuels*, 2025, **9**, 2982–2992.
9 A. S. Samarin, A. V. Ivanov and S. S. Fedotov, Toward Efficient Recycling of Vanadium Phosphate-Based Sodium-Ion Batteries: A Review, *Clean Technol.*, 2023, **5**, 881–900.
10 Y. Chen, Y. Shen, Z. Liu, M. Yang, Y. Zhang, Z. Niu, Y. Wang, M. Feng and Z. Shi, Natural Low-Melting Mixture Solvents for Green Recovery of Spent All-Solid-State Sodium-Ion Batteries with Superior Efficiency over Lithium-Ion Batteries, *ChemSusChem*, 2025, **18**, e202402457.
11 Y. Zhao, J. Zhang, Y. Wang, Y. Kang, H. Du, T. Jia, J. Xu, Y. Huang, F. Kang and B. Li, Cathode recycling of spent sodium ion batteries, *Energy Mater. Adv.*, 2024, **5**, 1–10.
12 Y. Chen, G. Zhao, J. Dong, J. Wang, D. Dong, Z. Li, M. Zhao, Z. Shi and Z. Niu, Green recovery of all-solid-state sodium-ion batteries/lithium-ion batteries by ionic liquids, deep eutectic solvents and low-melting mixture solvents, *Ind. Chem. Mater*, 2025, **3**, 464–474.
13 Y. Zhao, Y. Kang, J. Wozny, J. Lu, H. Du, C. Li, T. Li, F. Kang, N. Tavajohi and B. Li, Recycling of sodium-ion batteries, *Nat. Rev. Mater.*, 2023, **8**, 623–634.
14 Y. Chen, Y. Shen, Z. Shi, Z. Zhang, Q. Zhang, Y. Wang, M. Feng and C. Wang, Recovery of all-solid-state sodium-ion batteries cathode and solid electrolyte using deep eutectic solvents as green solvents, *Sep. Purif. Technol.*, 2025, **359**, 130473.
15 Y. Zhao, J. Zhang, Y. Wang, Y. Kang, H. Du, T. Jia, J. Xu, Y. Huang, F. Kang and B. Li, Cathode recycling of spent sodium ion batteries, *Energy Mater. Adv.*, 2024, **5**, 0128.
16 Y. Chen, M. Zhao, J. Chen, J. Dong, Z. Niu, T. Wang, C. Wang and Y. Zhang, Green Recovery of Toxic Prussian White Cathode From Spent All-Climate Sodium-Ion Batteries Using Low-Melting Mixture Solvents (LoMMSs), *Battery Energy*, 2025, **4**, e20240091.
17 Y. Chen and Z. Yu, Low-melting mixture solvents: Extension of deep eutectic solvents and ionic liquids for broadening green solvents and green chemistry, *Green Chem. Eng.*, 2024, **5**, 409–417.
18 N. Alomari, A. Maletta, S. Aparicio, A. Gutiérrez and M. Atilhan, Elucidating the dynamics behavior of PFASs at the water and hydrophobic low-melting mixture solvents interphase, *J. Mol. Liq.*, 2024, **407**, 125170.
19 X. Shen, L. Zhong, L. Li, B. Zou, H. Suo and L. Yan, Coupling chemical modification and immobilization of cellulase improves thermal stability and low-melting mixture solvent tolerance for in situ saccharification of bagasse, *J. Mol. Liq.*, 2024, **398**, 124253.
20 J. Niu, H. Wang, Z. Zhang, J. Li, Y. He and J. Hao, Efficient separation of cathode materials from aluminum foil by novel low-melting mixture solvent based on choline chloride-xylitol system, *Process Saf. Environ.*, 2024, **190**, 77–84.
21 P. Kalhor, Z. Sun and Z. Yu, Spectroscopic and Computational Study of $ZnCl_2$–Methanol Low-Melting-Temperature Mixtures, *J. Phys. Chem. B*, 2024, **128**, 2490–2503.
22 Y. Chen, Z. Shi, X. Zhang, C. Wang, Y. Wang, Z. Niu, Y. Zhang and M. Feng, Recycling Solid Electrolytes from All-Solid-State Lithium-Ion Batteries by Using Deep Eutectic Solvents as Green Extractants, *ChemSusChem*, 2025, **18**, e202402126.
23 Y. Chen, X. Zhang, C. Wang, Z. Shi, X. Wang, J. Dong, Y. Wang and M. Feng, Green recovery of solid electrolytes from all-solid-state lithium-ion batteries by low-melting mixture solvents with tunable physical properties, *Phys. Chem. Chem. Phys.*, 2025, **27**, 12004–12015.
24 Y. Chen, H. Liang, Q. Zhang, G. Zhao, Z. Liu, Y. Guo, Z. Yang, T. Wang and J. Chen, Simultaneously achieving high Li leaching efficiency and Li/Co selectivity from lithium-ion batteries cathode by using natural low-melting mixture solvents (LoMMSs) as green solvents, *Sep. Purif. Technol.*, 2025, **354**, 128967.
25 F. Zhou, Y. Tian, H. Zhang, Y. Yin, Z. Wang, R. Qin, Y. Chen, Z. Li and T. Mu, Enhanced Rapid and Efficient Recycling of Lithium-Ion Battery Cathode by Synergistic Effects of Ternary Deep Eutectic Solvents ChCl/MCl_x/Levulinic Acid, *ACS Sustainable Chem. Eng.*, 2024, **12**, 8090–18100.
26 Y. Chen, Y. Wang, Y. Bai, M. Feng, F. Zhou, Y. Lu, Y. Guo, Y. Zhang and T. Mu, Mild and efficient recovery of lithium-ion battery cathode material by deep eutectic solvents with natural and cheap components, Green, *Chem. Eng.*, 2023, **4**, 303–311.
27 Y. Chen, C. Liu, Y. Wang, Y. Tian, Y. Li, M. Feng, Y. Guo, J. Han and T. Mu, Efficient recovery of valuable metals from lithium-ion battery cathodes using phytic acid-based deep eutectic solvents at a mild temperature, *Energy Fuels*, 2023, **37**, 5361–5369.
28 Y. Zhang, B. Wang, F. Wang, Y. Dai, S. Ren, Y. Hou and W. Wu, A green recyclable process for selective recovery of Li and Fe from spent lithium iron phosphate batteries by synergistic effect of deep eutectic solvent and oxygen, *Sep. Purif. Technol.*, 2025, **354**, 128764.
29 M. K. Tran, M.-T. F. Rodrigues, K. Kato, G. Babu and P. M. Ajayan, Deep eutectic solvents for cathode recycling of Li-ion batteries, *Nat. Energy*, 2019, **4**, 339–345.